Supplementary Materials

Numerical Modeling of Shell-and-Tube-like Elastocaloric Regenerator

Žiga Ahčin, Parham Kabirifar, Luka Porenta, Miha Brojan and Jaka Tušek *

Faculty of Mechanical Engineering, University of Ljubljana, Aškerčeva 6, 1000 Ljubljana, Slovenia;
* Correspondence: jaka.tusek@fs.uni-lj.si

Graphical representation of the elastocaloric effect

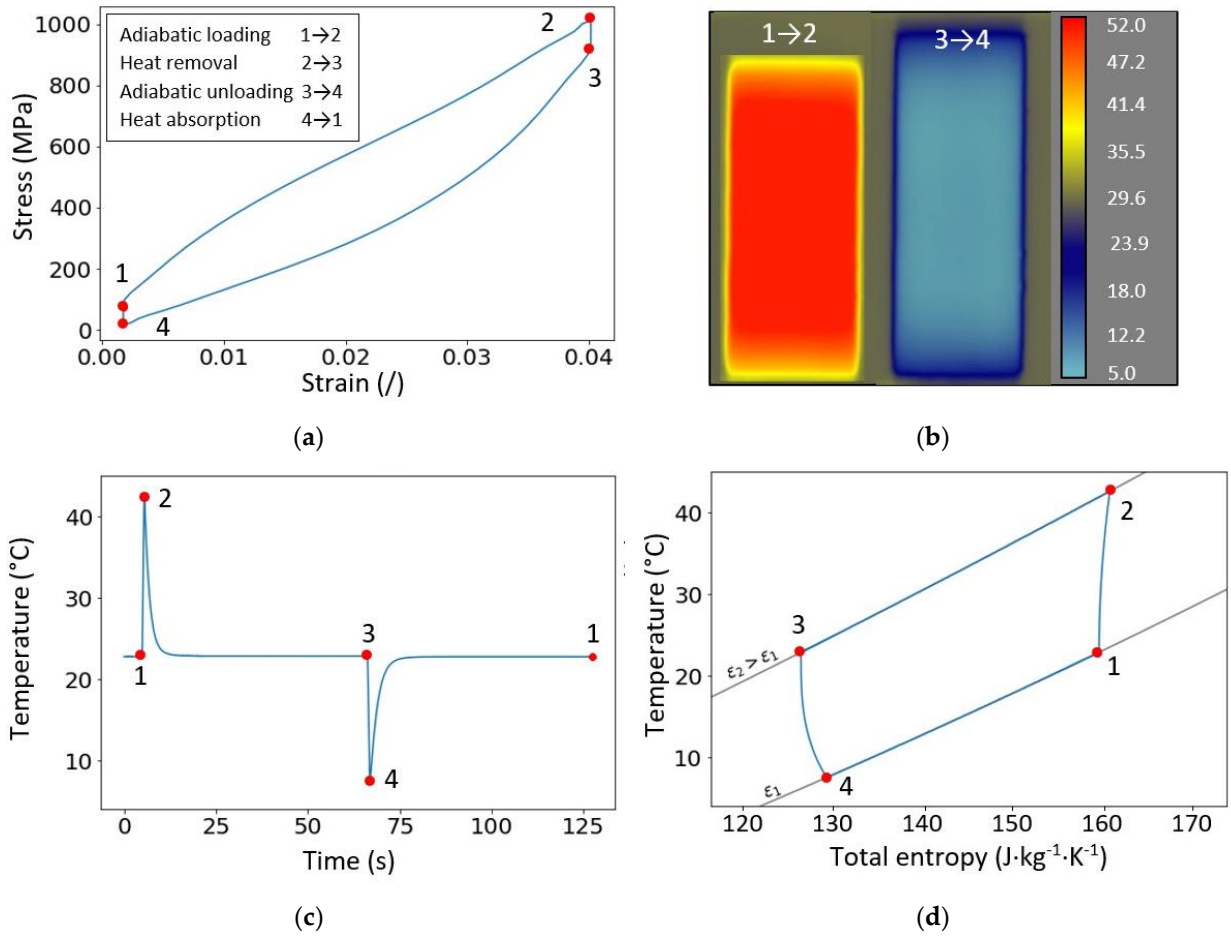

Figure S1: Graphical representation of the elastocaloric effect: superelastic stress-strain behavior during the superelastic/elastocaloric cycle (a); thermal imaging camera readings during adiabatic mechanical loading and unloading (b); temperature changes during the cycle (c); Brayton elastocaloric cycle in the T-s diagram (d).

Experimental setup for determining the superelastic and elastocaloric properties

Figure S2 shows the experimental setup used to determine the superelastic and elastocaloric properties of the NiTi tube. It consists of a primary and secondary lightning and a photo camera used for strain measurements. When the adiabatic temperature changes were measured, the photo camera was replaced with the IR camera. The sample (tube) is placed in the specially designed holder [1], which provides a uniaxial compressive loading.

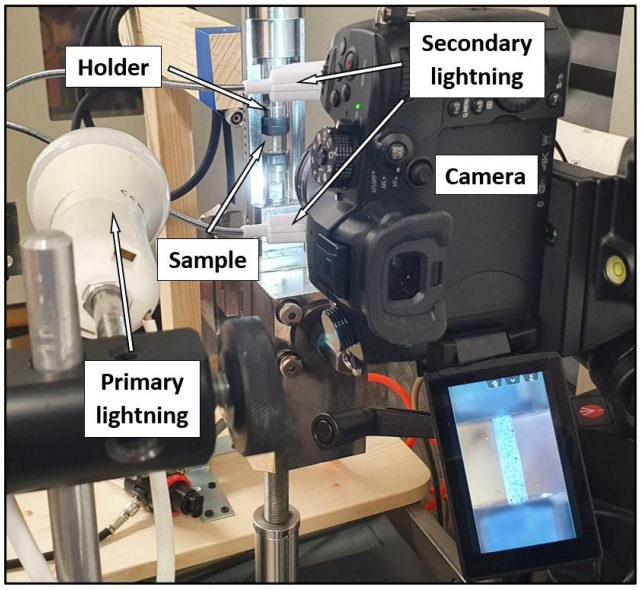

Figure S2: A photo of the experimental setup for determining the superelastic and elastocaloric properties of the Ni-Ti tube at room temperature

Isothermal stress-strain loops

Figure S3 shows the measured isothermal stress-strain curves at all four applied strains at two different temperatures. These results were used to calculate the hysteresis loop areas as a function of applied strain (see Figure 2 (d) in the main text).

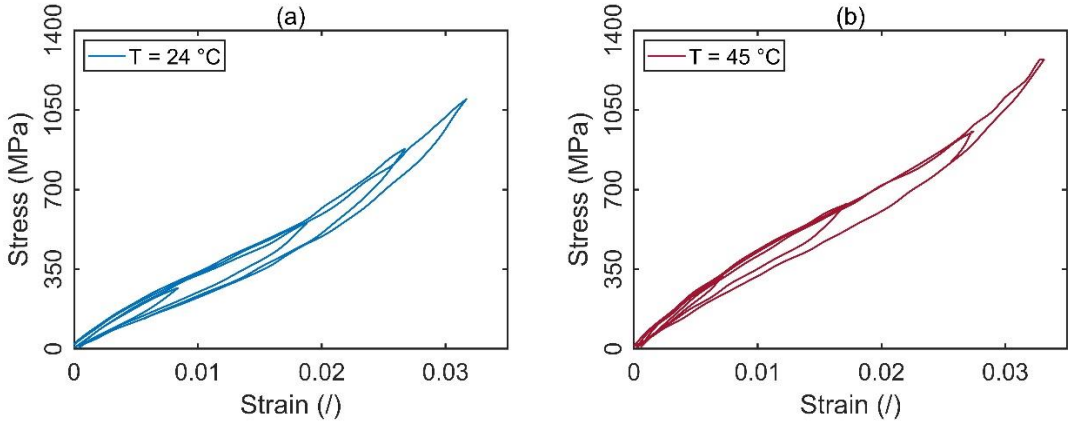

Figure S3: Measured isothermal stress-strain curves of NiTi tube at four applied strains at room temperature (a) and 45 °C (b).

Calculation algorithm

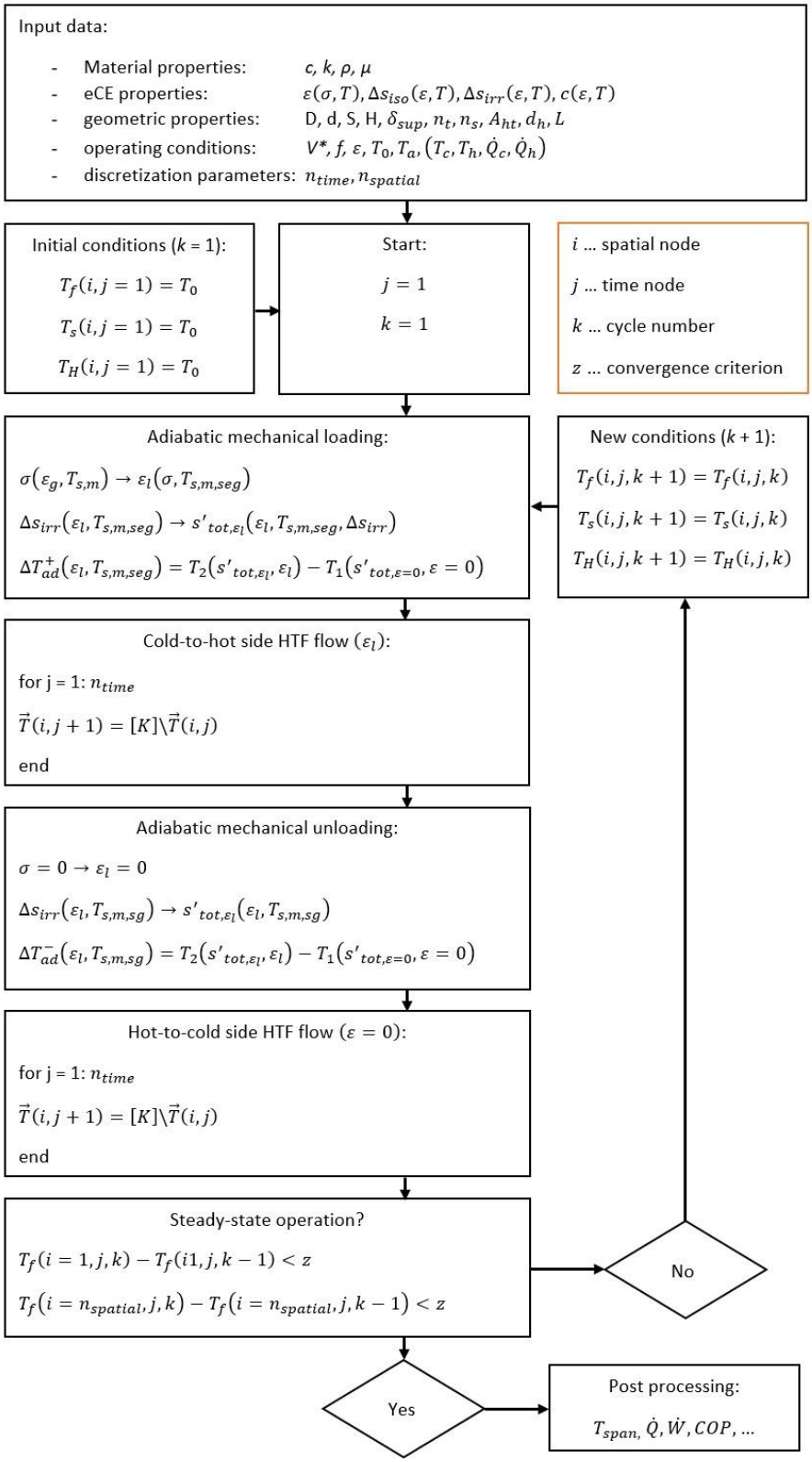

Figure S4: Flowchart of the numerical model of the AeCR.

Increase of tube diameter during mechanical loading

During cyclic loading and unloading, the tube diameter varies. The increase in tube diameter during loading was evaluated on a single tube under an applied strain of 3.2% using the Panasonic DC-GH5L camera. Figure S5 shows that the increase in diameter at the maximum applied strain was about 2.6%, and it is assumed that the increase in diameter has a linear relation with the applied strain. Therefore, the affected geometrical parameters (e.g., A_s, d_h) are calculated separately for loaded and unloaded AeCR (see Table A1 in Appendix A in the main text).

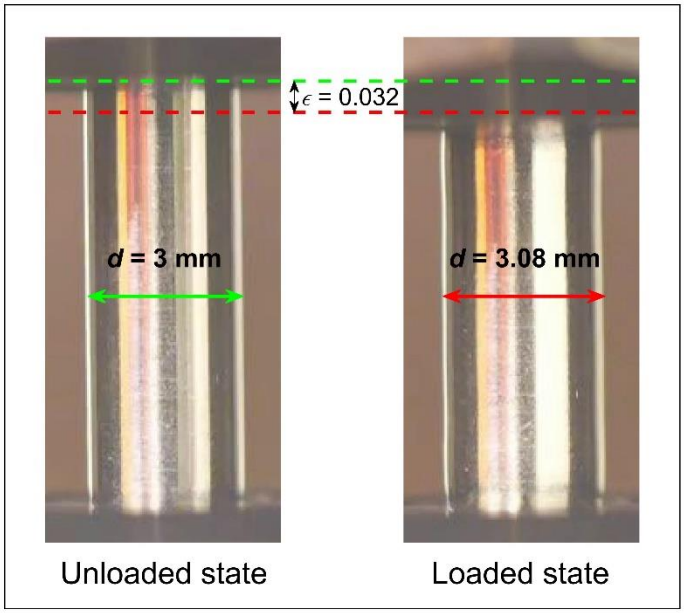

Figure S5: Comparison of the tube diameter in unloaded and loaded state (under applied strain of 3.2%)

Discretization error

The influence of the discretization parameters and the convergence criteria were evaluated to determine the parameters that provide sufficiently accurate results and acceptable computation times. For this purpose, COP was evaluated since it is most sensitive to discretization and convergence criteria. Figure S6(a) shows the influence of the convergence criteria on the calculated COP for three different operating conditions, where z = 0.0002 was chosen as a sufficient convergence criterion. Using this value as the convergence criterion, the influence of time and spatial discretization was further evaluated. Figure S6(b) shows the effect of the number of spatial and time steps (*m*) on the COP, based on which 200 spatial nodes and 400 time nodes were selected for further simulations.

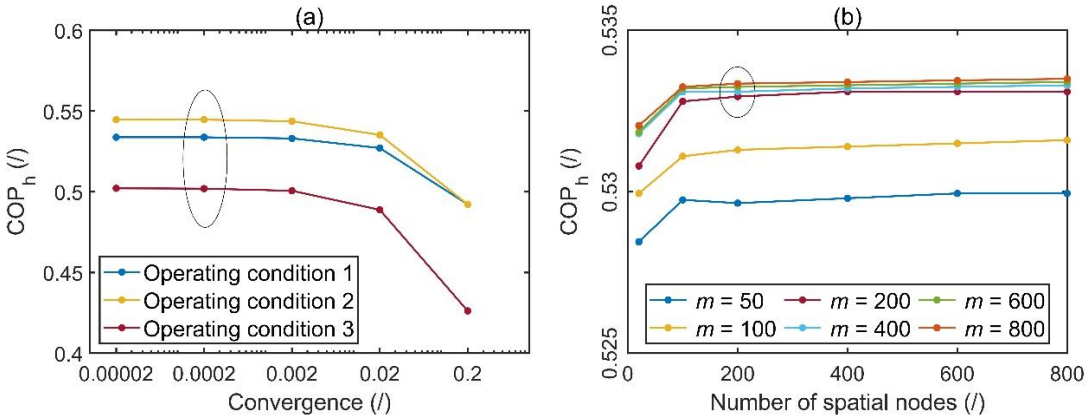

Figure S6: Influence of convergence criteria on the calculated COP (a); the influence of discretization parameters on the calculated COP (b).

Consistency of the numerical model

To evaluate the consistency of the numerical model, we compared the numerically calculated results (at zero temperature span of the AeCR) with the elastocaloric properties measured on a single NiTi tube. For this purpose, the heating/cooling power of the material (Equation S1), the mechanical input power calculated based on the stress-strain curves of the adiabatic tests (Equation S2), and the material COP_{mat} (Equation S3) were calculated based on the measurements on the single NiTi tube (see Section 2.1 in the main text for details on the experiments).

$$\dot{Q}_{mat} = m\, c\, \Delta T_{ad} f \tag{S1}$$

$$P_{mat} = V f \oint \sigma \, d\varepsilon \tag{S2}$$

$$COP_{mat} = \frac{\rho\, c\, \Delta T_{ad}}{\oint \sigma d\varepsilon} \tag{S3}$$

The numerical model was validated by comparing the cooling/heating performance of the AeCR (operating as a single-stage system at zero temperature span) with the experiments on a single NiTi tube. Figure S7 shows the contributions of the different effects on the AeCR performance in terms of heating power, input power, and COP. With the aim of comparing the AeCR performance with a single NiTi tube, the losses that occur in the AeCR other than hysteresis (i.e., heat exchange with the surroundings, longitudinal heat conduction, pressure losses, and the thermal mass of the housing and support elements) were neglected. In addition, a very large displaced volume ratio was used ($V^* = 10$), so it can be safely assumed that all the heat generated by the eCE is transferred to the HTF. The applied strain was set to the maximum strain reached during the experiments (2.7%) and the temperature was set to 24 °C. We can see from Figure S7 that under these assumptions, the measured values of the material's heating power, input power, and COP_{mat} agree relatively well with the ones calculated by the model (indicated with red color). The COP is slightly overestimated due to the larger modeled heating power and smaller modeled input power, which could be contributed to measurement and modeling errors. The COP_{mat} value under these operating conditions was experimentally determined to be 9.3. This value is slightly higher than the value determined in [2], where a clip-on extensometer was used on the tube holder itself. The extensometer strain measurements thus include both the friction between the holder and the tube, and the deformation of the holder. If we break down the available heating power, we see that most of the losses are due to heat losses to the surroundings, which account for almost 93% of all the losses (red highlighted area). Input power, on the other hand, is dominated by hysteresis losses, which account for 94% (green highlighted area) of the required input power. Similarly, the COP of the AeCR is most affected by the hysteresis losses (56% of the ideal COP), followed by the heat losses to the surrounding (17% of the ideal COP).

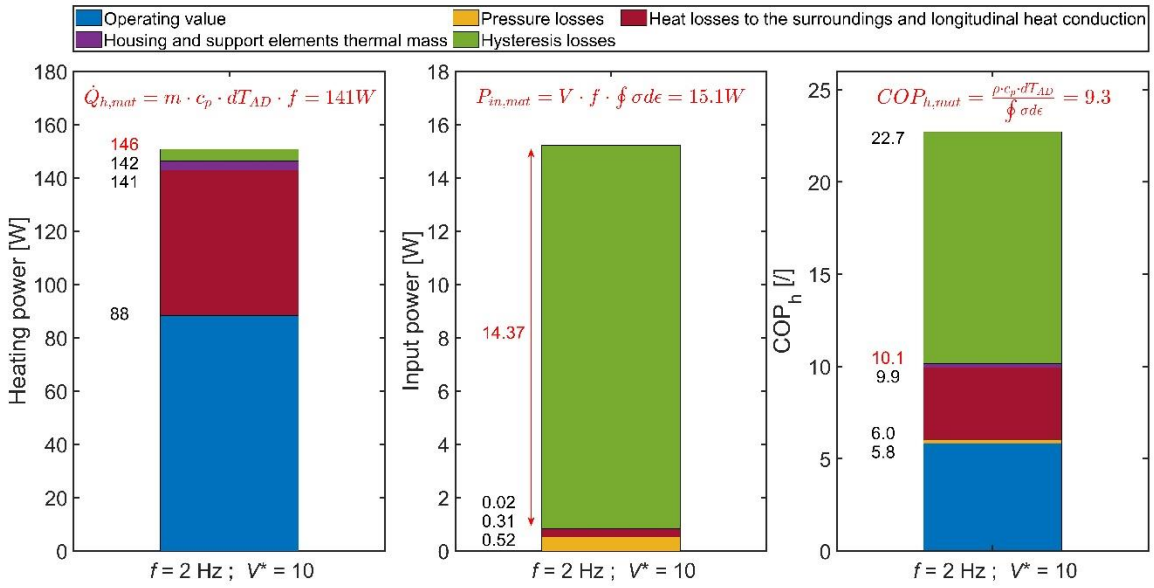

Figure S7: Comparison of modeled and measured material thermodynamic properties with the breakdown of the most influential losses of the AeCR.

Model verification against the experimental results at the stress level of 825 MPa

Here we present a comparison between the experimentally measured [3] and numerically calculated cooling and heating performance of the shell-and-tube-like AeCR at a stress level of 825 MPa (the comparison at 775 MPa is given in the main text, Section 3.1). Figure S6 shows a comparison between the measured [3] and the calculated maximum temperature spans established along the AeCR for the heat-pumping and cooling modes. As already explained in the main text, the numerical model predicts the maximum temperature span relatively accurately. However, larger deviations between experimental and numerical results are found when the AeCR operates at a smaller displaced volume ratio and a higher frequency, which could be related to the malfunction of the check valves at these operating conditions. Comparing Figure 7 from the main text and Figure S8, we find that increasing the stress results in a larger temperature span for all operating conditions due to the larger eCE. As explained in [3], due to the relatively high eCM austenite finish temperature of about -7 °C (above which reverse martensitic transformation is possible), the minimum operating temperature of the AeCR was limited to about 15 °C. This prevents the temperature of the eCM from falling below the austenite finish temperature at any stage of the cycle since the adiabatic temperature change during unloading can be as high as 20 K. Therefore, we could not perform experiments that would result in lower temperatures on the cold side of the AeCR, and thus the numerical simulations were not performed under these conditions.

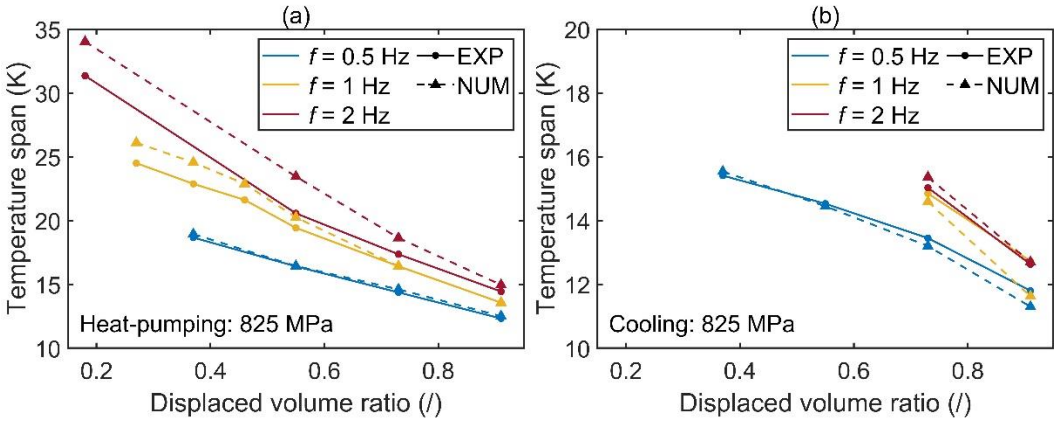

Figure S8: Comparison between the experimentally determined and numerically calculated maximum temperature spans established along the AeCR under different operating conditions for heat-pumping (a) and cooling (b) at the stress level of 825 MPa.

Figure S9 shows a comparison between the experimentally determined and numerically calculated temperature span – cooling/heating power characteristics at a stress level of 825 MPa. Here, the operating frequency was kept constant at 2 Hz while the effects of three different displaced volume ratios were evaluated. At smaller displaced volume ratios, the numerical model slightly overestimates the AeCR performance, while at larger displaced fluid volume ratios, the experimental results are underestimated to some extent, but the general trend of dependency is predicted correctly.

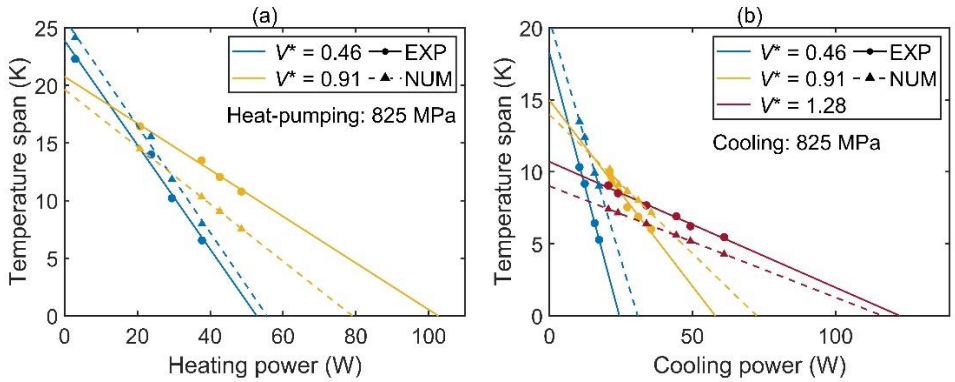

Figure S9: Comparison between experimentally determined and numerically calculated temperature span – cooling/heating power characteristics for heat-pumping (a) and cooling (b) at the stress level of 825 MPa.

Figure S10 shows a comparison between the experimentally measured and numerically calculated COP values at a stress level of 825 MPa, where we can see that the numerical model slightly overestimates the experimentally determined COP. This is somewhat different from the case of 775 MPa (Figure 9 in the main text), where the numerical model underestimates the measured COP values. The reason for this might be related to larger friction between the tubes and the baffles at the stress level of 825 MPa compared to 775 MPa. Namely, the numerical model considers the mechanical input work based on the hysteresis (i.e., stress-strain characteristics) measured on a single tube, while the experimentally measured mechanical input work includes other effects, such as the friction between the tubes and the baffles and the deformation of the housing (e.g., steel plates and PEEK insulation at both ends [3]). Under mechanical loading, the tube diameter increases, which increases the friction between the tubes and the baffles, and this can lead to a somewhat larger measured hysteresis and thus a larger input work compared to the numerically calculated input work, especially at higher stress levels where the friction is more pronounced.

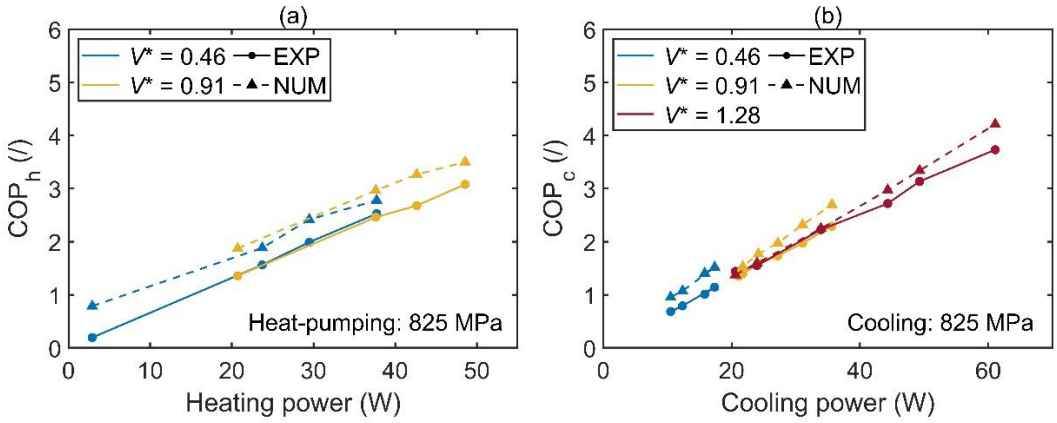

Figure S10: Comparison between the experimentally determined and numerically calculated COP – cooling/heating power characteristics for heat-pumping (a) and cooling (b) at the stress level of 825 MPa.

References

1. Porenta, L.; Trojer, J.; Brojan, M.; Tušek, J. Experimental investigation of buckling stability of superelastic Ni-Ti tubes under cyclic compressive loading: Towards defining functionally stable tubes for elastocaloric cooling. *Int. J. Solids Struct.* **2022**, *256*, 111948. https://doi.org/10.1016/j.ijsolstr.2022.111948.
2. Porenta, L.; Kabirifar, P.; Žerovnik, A.; Cebron, M.; Žužek, B.; Dolenec, M.; Brojan, M.; Tušek, J. Thin-walled Ni-Ti tubes under compression: Ideal candidates for efficient and fatigue-resistant elastocaloric cooling. *Appl. Mater. Today* **2020**, *20*, 100712. https://doi.org/10.1016/j.apmt.2020.100712.
3. Ahčin, Ž.; Dall'Olio, S.; Žerovnik, A.; Baškovič, U.Ž.; Porenta, L.; Kabirifar, P.; Cerar, J.; Zupan, S.; Brojan, M.; Klemenc, J.; Tušek, J. High-performance cooling and heat pumping based on fatigue-resistant elastocaloric effect in compression. *Joule* **2022**, *6*, 2338–2357. https://doi.org/10.1016/j.joule.2022.08.011.